Reactive Behavior of the $[LiH_2]^+$ System II. Collision-Induced Dissociation and Collinear Reaction Dynamics of LiH^++H from Quantum Time Dependent Calculations

E. Bodo,[†] F. A. Gianturco,*[,†] and R. Martinazzo[‡]

University of Rome "La Sapienza", Department of Chemistry, P.le Aldo Moro 5, 00185, Rome, Italy, and University of Milan, Department of Physical Chemistry and Electrochemistry and CNR center CSR SRC, V. Golgi 19, 20133, Milan

Received: June 19, 2001; In Final Form: October 12, 2001

The time-dependent approach to reactive scattering is applied to the study of the collinear collisions for the LiH^++H system. The reaction LiH^++H → H_2+Li^+ is adiabatically confined to the ground electronic state of the LiH_2^+ system and is highly exoergic (∼4.2 eV). However, despite the strong energetic gain, the present calculations show that the reactive component is only a negligible outcome of the encounters while the simple inelastic scattering process and the collision-induced dissociation dominate the dynamics. The binding energy of the LiH^+ reagent molecule is so weak that the threshold of the triatomic dissociation channels becomes open at a collision energy of only a few tenths of an electronvolt. The total dissociation probabilities are obtained via an accurate computation of all the possible bound-to-bound transition probabilities (reactive and nonreactive) using the quantum time-dependent approach described herein.

1. Introduction

The LiH molecule is one of the few molecular species that is supposed to have a role[1−7] in the chemistry of the primordial universe environment, at least in the standard nucleosynthesis framework where elements heavier than Be are not present. The LiH molecule is known to be present at a very low concentration with respect to more abundant molecules such as H_2, H_2^+, or HeH^+, as it results from kinetics models of the primordial chemistry which are based on an ensemble of rate constants that are mostly crude estimates obtained from enthalpic considerations.[8,9] The work that has been carried out in our group in the past few years has provided us with a considerable amount of new results on the electronic structures and on the dynamical behavior of systems such as LiH−H and $[LiH-H]^+$. In particular, in two recent papers[10,11] we showed how, starting from an accurate analysis of the topology of the interaction potentials, the current landscape of the lithium chemistry in a primordial environment has to be severely modified to correctly account for the low probability of some of the involved reactions to actually occur. In particular, we showed how reactions such as the charge-transfer process ($LiH+H^+$ → LiH^++H), are adiabatically forbidden and extremely unlikely in a environment (such as that of the primordial universe) where three-body collisions or photochemical reactions are negligible. Part of those results are published in the preceding paper (hereafter referred to as paper I) and in ref 11.

Such considerations have driven us to start an accurate study of the dynamical processes taking place in the ionic system LiH_2^+, while for the neutral LiH_2 we defer the interested reader to the existing literature.[12−14] As explained in detail in paper I, the LiH_2^+ ensemble presents marked differences between the chemical and dynamical behavior of its first two electronic states. The ground electronic state correlates, in fact, with LiH^+-($^2\Sigma^+$) + H(^{1}S) on one side and with $H_2(^1\Sigma^+)$ + $Li^+(^1S)$ on the other (we are considering here, and throughout this work, only the attractive singlet state of the global LiH_2^+ system). The first excited state, instead, breaks up into $LiH(^1\Sigma^+)$ + $H^+$and $H^+_2(^2\Sigma^+)$ + Li(^{2}S). If we examine more accurately the topology and the electronic structure of the collinear reactive PES, as done in paper I, we can safely exclude the role of nonadiabatic interactions between the two states and thus focus our attention on the following reactions:

$$LiH^+ + H \rightarrow H_2 + Li^+ \quad (1)$$

$$LiH + H^+ \rightarrow H_2^+ + Li \quad (2)$$

Here we will consider first the ground-state reaction, while the excited-state process, as explained in paper I, will be analyzed elsewhere in conjunction with the study of the rotovibrational excitation/deexcitation in LiH by proton impact.[15]

2. The Reactive Potential Energy Surface

For the collinear geometries that we are starting our analysis with, the scattering problem is easily worked out using the usual mass-scaled Jacobi coordinates[16] (in the following, Q_1 will be the translational reagent coordinate and Q_2 the vibrational one). The two surfaces in these skewed coordinates for the ground electronic state of the two collinear geometries Li−H−H (at a Jacobi angle of 0°) and H−Li−H (180°) are reported in Figure 1. In the left panel we report the contour plots obtained using our fitting of the ab initio points for the Li−H−H geometry, while in the right one a similar fitting procedure produced the potential energy surface displayed for the H−Li−H geometry. The details of the calculations were given in paper I.

As it is clear from Figure 1, the two directions of approach of the H projectile are markedly different simply because only the 0° orientation can lead to the formation of H_2. This geometry shows a extremely exoergic pathway that is due to the large difference in the binding energies between products and

* Corresponding author.
[†] University of Rome.
[‡] University of Milan.

10.1021/jp012344x CCC: $20.00
Published on Web 11/16/2001

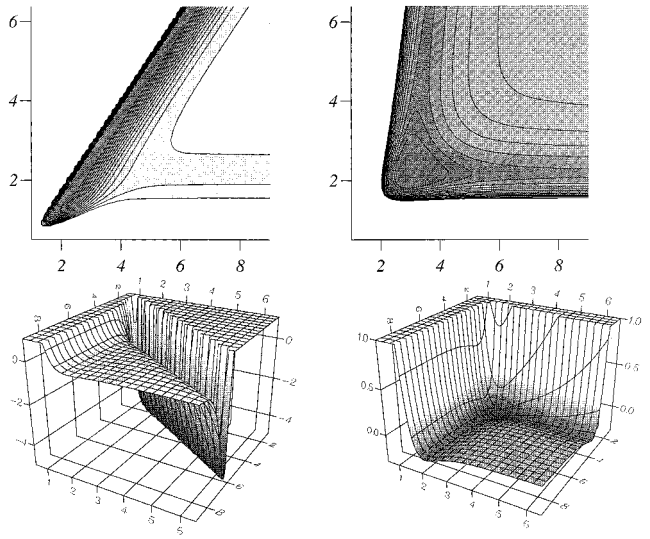

Figure 1. The two reactive PESs for the collinear collisions Li−H−H (left) and H−Li−H (right) in the ground state. On the left the energy ranges from −5.0 eV to 1.0 eV while on the right from −0.5 eV to 0.5 eV. In the upper panels the abscissae correspond to the mass scaled translational [LiH]−H coordinate (Q_1), while the ordinates give the mass scaled vibrational [Li−H] coordinate (Q_2) (both distances are in Å).

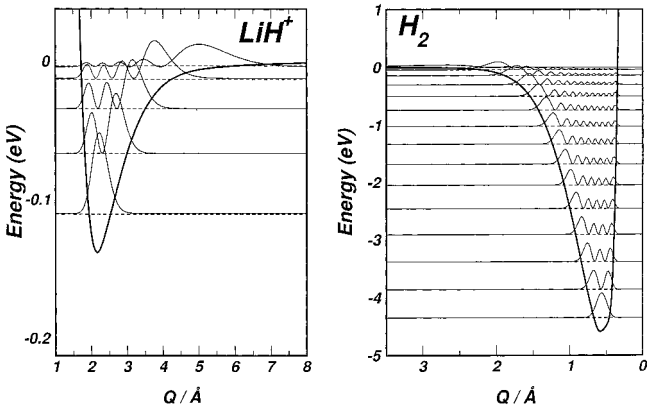

Figure 2. Asymptotic potentials of LiH^+ (left) and H_2 (right) referred in their respective dissociation limits as a function of mass-scaled internal coordinates. Also, the vibrational levels are displayed with the square of the wave functions.

reactants, as one can easily see in Figure 2 where we report the asymptotic potential profiles for LiH^+ and H_2 with their vibrational levels and density probabilities. The LiH^+ molecular ion with its low binding energy ($D_e = 0.138$ eV), supporting five bond vibrational levels, has to be compared with the molecular structure of H_2 with 15 bond vibrational levels. Taking into account the ZPE, the exoergicity of the reaction results to be 4.241 eV. Another striking aspect of the PES is the narrowness of the product channel, a feature that, as we shall see below, will strongly influence the dynamics. This is due to both to the electronic structure of the HH bond and to the light nature of the nuclei involved. The skewing angle (i.e., the $tg^{-1}(m_H/\mu)$, with μ being the total reduced mass of the system) that characterizes this surface is 48.6° because of the external position of the Li atom.

A completely different situation occurs when the H atom impinges on the other side of the molecular ion: in this case the surface is indeed clearly symmetric (almost flat) and with a shallow well due to the relatively weak polarization interaction between LiH^+ and H. In this case the skewing angle is of 82.8° degrees because this time the exchanged atom is the heavier Li.

3. Computational Method

As one can see from Figure 2, the triatomic dissociation threshold is very low, due to the small binding energy of LiH^+, and thus the triatomic dissociation channel becomes open at a very low collision energy (0.111 eV for the ground vibrational level). As is well known, the presence of reactive and dissociative channels within the same range of energies poses some conceptual and pratical problems in treating the dynamics. These are, in fact, mainly due to the presence of a nonorthogonal double continuum associated with the full break-up. Indeed, the continuum eigenfunctions of the LiH^+ are needed to describe both the reaction forming H_2 and the full triatomic dissociation process.[17]

The presence of the double continuum requires that one could resort to using hyperspherical coordinates to correctly describe on equal ground both the dissociative and "reactive" continua, using a basis set constructed of asymptotic states. Indeed, most of the previous studies on the collision-induced dissociation involved a time independent scheme in hyperspherical coordinates that rely on a DVR representation of the scattering eigenfunction with the proper boundary conditions. In these previous studies (where one reactive channel is also present) only the collinear geometry has been investigated.[18−21] When the reactive arrangement can be neglected, instead, a full 3D calculation becomes feasible: both a semiclassical[22,23] and a quantum mechanical (IOS) description have been applied[24−26] to simple systems such as $He+H_2$. The approach has the advantage of giving a complete description of the scattering process, thereby yielding the relevant S matrix, but it should be mentioned that in the hyperspherical coordinates the propagation can be inefficient and time consuming for a multichannel problem.[27−29]

Since we are not interested in the kinetic energy distributions of the three atoms, a complete grid description of the wave function is sufficient to obtain the *total* dissociation probabilities by computing all the bond-to-bond probabilities. The calculations have been carried out using the well-known method of time-dependent scattering theory.[30] Since the time-dependent quantum mechanical methodology is well documented in the existing literature, only specific details concerning the present numerical implementation will be discussed here.

The initial wave function was taken to be the product of a minimum-uncertainty Gaussian wave packet for the relative translational motion and a vibrational eigenfunction of LiH^+ obtained by a Numerov integration of our asymptotic Hamiltonian. The initial wave packet, located well into the reagent asymptotic region (∼10 Å), has been chosen narrow enough to allow us to examine a wide range of collision energies with a single propagation, without loosing accuracy in the representation of it on the chosen spatial grid. In particular, we have employed seven different wave packets (see Figure 3), each with a mean linear width of $\delta x = 0.125$ Å, except for the lowest energy for which the width was chosen to be 0.27 Å so as to have only momentum components directed toward the interaction region. The lowest energies considered are those at the triatomic dissociation threshold (as one can see in the inset in Figure 3), while all the other wave packets are confined to energy regions above the dissociation threshold.

The time evolution of the wave packet was carried out using the usual split operator method[31] combined with the fast Fourier transform (FFT) algorithm to evaluate efficiently the action of

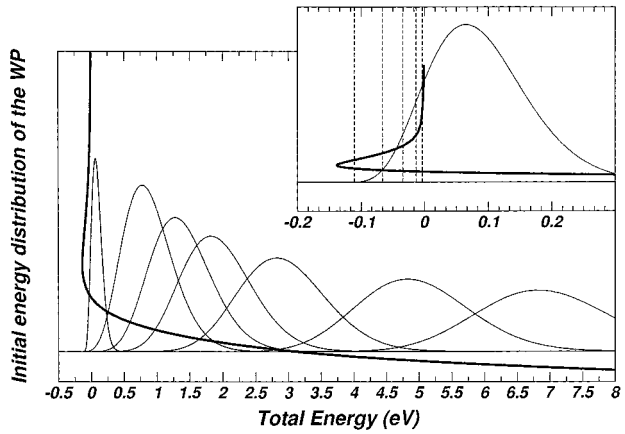

Figure 3. Distribution of energies for the seven wave packets used in the calculations. The energy scale is the total energy with respect to the dissociation threshold of the three atoms. The thick solid line is the asymptotic potential of LiH^+. The inset shows the well region of the latter molecule with its bound vibrational level.

the kinetic energy part of the Hamiltonian on the wave function. The grid had to be dense enough to adequately represent all momentum components in the wave packet. In particular we had to correctly represent the large energy gain due to the deep well (∼4 eV) in the product region together with the collision energy. We therefore used different grid spacings depending on the collision energy: the largest one was built of 384 points in 14 Å for the Q_1 coordinate (from 1 to 15 Å) and of 256 points in 8.5 Å for the Q_2 coordinate (from 0.5 to 9 Å). These parameters are sufficient to represent up to 20 eV in the entrance channel and up to 37 eV in the product channel.

The propagation was carried out using a very short time step (0.01 fs) to correctly account for the large potential energy difference experienced by the wave packet when it enters the product channel. The calculation was continued until 0.01% of the wave function was absorbed by the absorbing potentials placed at the grid boundaries. The absorbing potentials used were two cubic ramps of the functional form

$$V_{\mathrm{NIP}} = \begin{cases} -\mathrm{i}V_0\left[\dfrac{-q_{\mathrm{N}} - \Delta q}{\Delta q}\right]^3 & q_{\mathrm{N}} - \Delta q \le q \le q_{\mathrm{N}} \\ 0 & \text{elsewhere} \end{cases} \quad (3)$$

where q represents any linear coordinate, q_{N} is the boundary point of the grid, and Δq is the width of the absorbing region. V_0 was set to the value of the mean kinetic energy of the wave packet, and the spread of the absorbing potential was set to 5 Å along Q_1 and to 3 Å along Q_2. All the parameters used here have been chosen after several test calculations and represent stable solutions for all the considered dynamical quantities.

3.1. Bond-to-Bond and Total Dissociation Probabilities. In principle a complete grid representation of the wave function should not suffer the problems associated with the existence of a double continuum, and thus it should be possible to extract total dissociation probabilities from a 2D time-dependent calculation. One can, in fact, calculate the $i \rightarrow f$ state-to-state probability, $P_{f\leftarrow i}$, using the usual time−energy mapping (see Chapter VII of ref 30)

$$\left|\int_0^\infty \mathrm{e}^{iEt}\langle R^\infty f|\psi_{\mathrm{t}}^{(\mathrm{i})}\rangle\, \mathrm{d}t\right|^2 = 2\pi\mu^2 a_E\, \mathrm{P}_{f\leftarrow i}(E) \quad (4)$$

Here $|\psi_t^{(i)}\rangle$ is the wave packet at time t (initially prepared in state i), $|f\rangle$ is an asymptotic eigenfunction of the products (or of the reagents), and $|R^\infty\rangle$ is a Dirac delta function of the scattering coordinate in the product (reagent) arrangement, located well into the asymptotic region, so that the spatial integral in eq 5 is actually to be performed on a dividing surface (on a line for 2D) well into the relevant asymptotic region. As usual,[30] the quantity a_{E} is the weight of the energy component E in the initial wave packet. If one chooses to represent the wave packet in the *reagent* skewed coordinates, the calculation for the subreactive transitions is easily accomplished. For the product transitions, however, one has to transform the wave function into the mass-scaled Jacobi coordinates of the products before evaluating the spatial integral of eq 5. Hence, we interpolate the wave function values on the original grid points by using the Fourier-based DVR basis set implicitly assumed in our calculation: the wave function at a given point $A(Q_1, Q_2)$ can in fact be obtained by

$$\psi(A) = \sum_p^{N_1N_2} \psi(Z_{\mathrm{p}})\xi_{\mathrm{p}}(A) \quad (5)$$

$Z_p(Q^p{}_1, Q^p{}_2)$ is a point of the skewed grid, N_1 and N_2 are the grid dimensions, and the basis functions are

$$\xi_{\mathrm{p}}(A) = \frac{1}{(N_1L_1)^{1/2}} \frac{\sin\left\{\dfrac{(N_1 - 1)\pi(Q_1 - Q^p{}_1)}{L_1}\right\}}{\sin\left\{\dfrac{p(Q_1 - Q^p{}_1)}{L_1}\right\}} \frac{1}{(N_2L_2)^{1/2}} \frac{\sin\left\{\dfrac{(N_2 - 1)\pi(Q_2 - Q^p{}_2)}{L_1}\right\}}{\sin\left\{\dfrac{(Q_2 - Q^p{}_2)}{L_2}\right\}} \quad (6)$$

with L_1 and L_2 being the length of the grid. Thus, we can represent the wave function over a line sufficiently far from the interaction region and which coincides with the vibrational coordinate of the products. It is worth noting at this point that the contribution from the various basis functions defined by eq 7 is very localized in space, and thus we evaluate the wave function at a given point A (on the product analysis line) summing up in eq 6 only the contributions from the points Z contained in a square centered in A. The size of the square was limited to the first nearest 100 grid points. Different test calculations have been carried out to correctly place the analysis line and to determine the optimal length and spacing of it. We used a sufficiently long line to correctly represent the highest vibrational wave function of H_2, and the grid spacing used in the evaluation of the integral in eq 5 was taken to be comparable to that of the two-dimensional grid. We checked the numerical stability of the final transition probabilities to changes in the parameters that characterize the analysis line by preparing a wave packet in the exit channel as a superposition of vibrational functions of the products and evolving it in time toward the asymptotic region.

This rather involved procedure is necessary because the common flux approach,[30] normally used to yield directly the total reaction probabilities, fails when the triatomic dissociation is an open channel. This break-down occurs because the reactive flux going through a chosen dividing surface would also include the dissociating flux going through that same surface. Indeed, total reaction probabilitites calculated with the flux approach are very sensitive to the position of the dividing surface, even in the absence of inelasticity in the product channel.

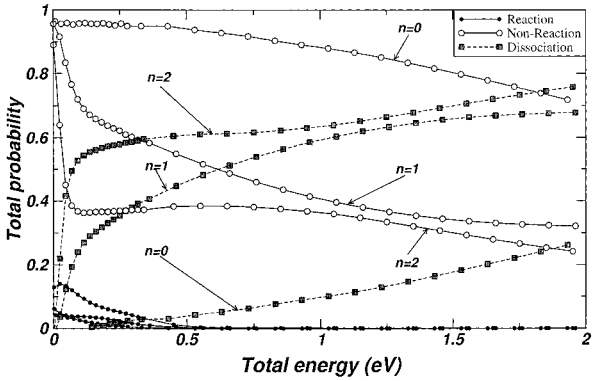

Figure 4. Total probabilities for the three possible processes at low energy (above dissociation threshold) as a function of total energy (see text). The three sets of curves refer to the lowest three vibrational levels of LiH^+.

The correct evaluation of the reactive and, simultaneously, of the nonreactive transition probabilities (that we call here bound-to-bound transitions) allows us to have the *total* dissociation probabilities as given by

$$P_n^{\mathrm{CID}}(E) = 1 - (P_n^{\mathrm{R}}(E) + P_n^{\mathrm{NR}}(E))$$

where n is the initial vibrational level and P_n^{R} and P_n^{NR} are the total reactive and nonreactive transition probabilities (i.e., summed over all the final vibrational states of the product and of the reagent, respectively).

4. Results and Discussion

4.1. The Collinear Reaction Li−H−H. The first geometry that we sampled is the one that should be the most likely for the reaction $LiH^+ + H \rightarrow H_2 + Li^+$ to happen (the Jacobi angle is $\theta = 0°$). As previously mentioned in this paper, the energy profile is extremely exoergic (∼4.2 eV) and thus one should expect a fast conversion of LiH^+ into H_2, but, as we shall see below, the impact of the wave packet on the repulsive wall opposite the reagent channel will instead preferentially break up the initial diatom LiH^+. Indeed, the motion of the wave packet is very simple and consists of two successive impacts, the first on the H_2 repulsive wall and the second on that of LiH^+. The wave packet then returns to the reagent side, having become more widely spread in space due to the CID process (see below).

To better clarify the above point, we report in Figure 4 the total probabilities for the three processes that can take place just above dissociation threshold. For each process we show the results obtained with an initial state being prepared in each of the first three vibrational levels of the reacting molecules. The filled-in circles are reaction probabilities, the open circles are the subreactive probabilities, and the filled-in squares are the dissociation probabilities. For a wave packet prepared in the ground vibrational state, the subreactive process (i.e., the permanence of a bound LiH^+ after the collision) is dominant, although an increase in energy tends to also increase the dissociation products. Here we see that the threshold is not specifically defined for $n = 0$ since the energy threshold does not coincide with the dynamical one, as already noted in previous works (see, for example, ref 32 and reference therein). A marked enhancement of the dissociation process when LiH^+ is prepared in a vibrationally excited state is clearly evident in the figure: the dissociation is the dominant process both for $n = 1$ and $n = 2$, already at a fraction of an eV above threshold.

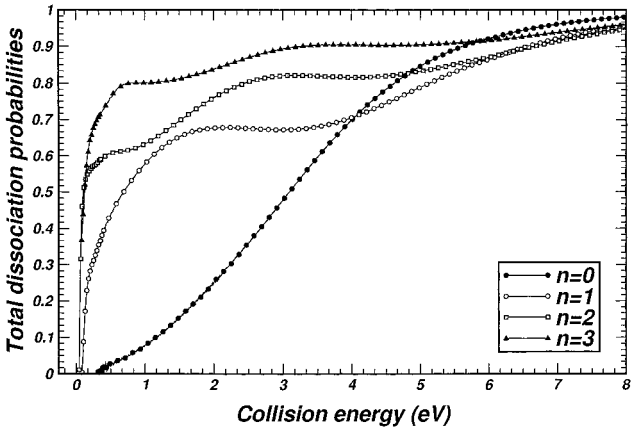

Figure 5. Total collision induced dissociation (CID) probability as a function of collision energy for the first four initial vibrational levels of LiH^+.

The most striking result is given by the almost complete absence of reaction (filled-in circles in Figure 4), even when the energy is just above the threshold (0.1−0.5 eV). The highest reaction probabilities are observed for the $n = 2$ initial vibrational level, but they still do not exceed 20% of the total and decrease rapidly with increasing total energy. The absence of reactive contributions is probably due both to the narrowness of the potential well where the products are formed and to the reduced vibrational inelasticity of the exit channel, a feature that makes the products unable to absorb efficiently the release of excess energy.

If we now look at the dissociation probabilities as a function of the collision energy over a broader range (Figure 5), we clearly identify the thresholds corresponding to the different initial vibrational energies and, for collision energies below 4 eV, we can see the effect of the vibrational enhancing due to the "heating" of the reagents. For higher energies the vibrational excitation of the reagent is not any more the driving force of the break-up process, and a vibrational quenching is observed instead. One striking feature of the curves shown in Figure 5 is the presence of marked shoulders, already noted by several authors before (e.g., see ref 32 and references therein) in systems where there are no rearrangement channels. The presence of these shoulders in our case appears to be linked to the dynamical absence of reaction during the collisional event. We point out that the number of such shoulders is equal to the vibrational quantum number of the initial wave packet. This seems to be an indicator of direct dynamics taking place on this very simple potential energy surface. Indeed, when one looks at the final wave packets, one clearly notes a sort of memory effect of the initial vibrational state. As shown in Figure 6, the wave packet spreads in space because of the dissociation process but preserves the initial nodal structure of the molecular bound state selected for the process. The discrete contribution of each lobe of the wave packet to the break-up flux seems to be responsible for the previously mentioned structured CID probabilities. It would be interesting to see if such structure will also be preserved when the full dimensionality of the problem is taken into account.

We have already mentioned that most of the flux after the reactive event is shared by the subreactive and the dissociation channels. The subreactive channels leave the LiH^+ with a vibrational population spread over its entire vibrational spectrum. This could appear strange at first because it is not commonly found that the nodal structure of the bound reagent wave functions is being preserved during the collision but, as it should

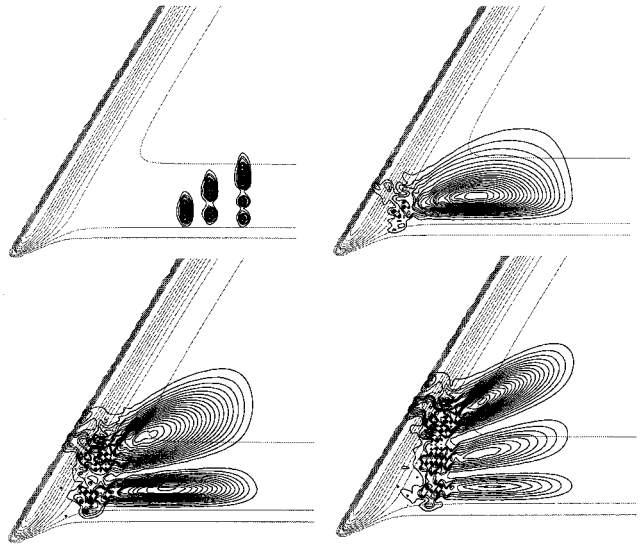

Figure 6. Initial and final stage of the evolution of the probability density for a wave packet prepared in the first three vibrational levels of LiH^+. In the upper panel on the left we have the initial situation for the three different wave packets (shifted in Q_1 for clarity) and in the remaining panels the situation soon after the collision (90 fs) for a mean kinetic energy of 1.0 eV.

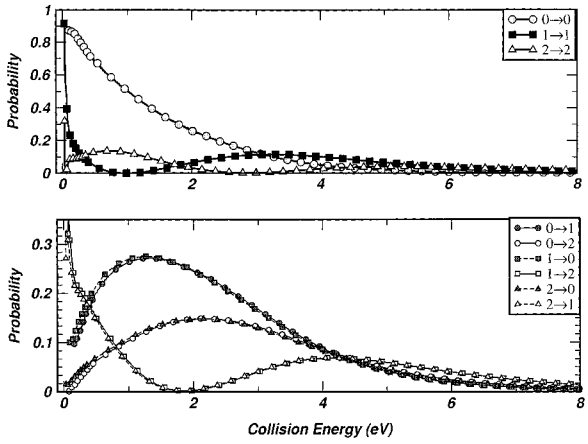

Figure 7. Subreactive probabilities as a function of collision energy. Upper panel for the elastic transition, lower panel for the inelastic vibrational excitations and relaxations. For clarity of presentation only transitions for $n < 3$ are reported.

be clear from Figure 6, the probability density is strongly distorted by the effect of the repulsive wall and is pushed outward with respect to the initial situation. The effect of this sudden feature in the dynamics can be seen when one looks at the subreactive state-to-state transition probabilities for the first three vibrational levels reported in Figure 7. In this figure, both the elastic and inelastic transition probabilities show oscillations as a function of energy before being suppressed by the increasing dominance of the dissociative event. These oscillations seem to be the imprints of the various lobes of the final wave function going through the asymptotic region of the bound LiH^+. The final wave function is increasingly more spread out in space by the impact with the repulsive wall of H_2 as the energy increases. The oscillating patterns in the state-to-state transitions therefore give rise to the shoulder structure in the total CID probabilities because of the absence of reactive contribution at those energies. The nondiagonal transition probabilities in the lower panel of Figure 7 satisfy the microreversibility principle

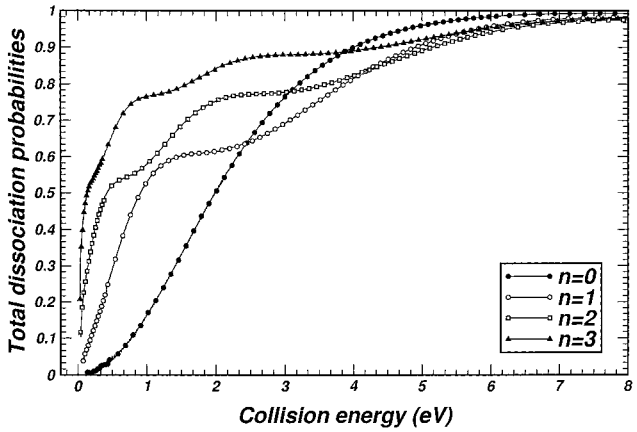

Figure 8. Collision-induced dissociation probabilities for the H−Li−H orientation. See Figure 5.

(the vibrational energy is quite low on such a scale), although they come from the time evolution of different wave packets, thereby providing a check of the accuracy of our calculation.

4.2. The Collinear Reaction H−Li−H (θ = 180°). The second geometry considered here is that with a Jacobi angle of $\theta = 180°$, i.e., $[H-H-Li]^+$ where the possible reaction is degenerate and is given by $H_a + LiH_b^+ \rightarrow H_aLi^+ + H_b$. For this reason, the surface reported in Figure 1 exhibits a shallow well and does not show the deep well of the previously investigated orientation. We have chosen to perform an analogous set of calculations in this arrangement to see if the pattern for the collision-induced dissociation remained similar to the one already found for the other approach. Although not entirely sufficient, this further test could help us to more clearly understand if a three-dimensional calculation could lead to similar results, at least for the general behavior of the dynamics.

In Figure 8 we report the results for the collision-induced dissociation probabilities in a manner similar to that of Figure 5. As one can see, the results do not change much in this new orientation. The physical picture of a reactive dynamics dominated by CID processes is mantained. Such a test helps us to render more realistic the assumption that all the properties of the dynamics are determined by the interaction of the wave packet with the repulsive wall, which is chiefly created by the H_2 potential above dissociation. Also, in this case the total flux is shared between the dissociative and the subreactive events. This is why we can observe in Figure 8 the same shoulder structures seen before in Figure 5. In the latter case, the structure is even more evident showing here a perfect correspondence with the initial vibrational states up to the $n = 3$ level.

4.3. The Effect of Isotopic Variations. One of the interesting results of the above analysis is that, even in the most favorable orientation Li−H−H, the collision does not lead to the production of an appreciable quantity of H_2. The specific shape of the PES discussed in detail in paper I allowed us to suggest that such a behavior was due to the particularly narrow shape of the H_2 exit channel. To further check this prediction, we consider here the effect of an enlargement of the well in the exit channel, which arises from the mass changes from the isotopic substitutions in the mass-scaled coordinate system. Two kinds of isotopic substitution have been examined: $LiD^+ + H \rightarrow Li^+ + DH$ and $LiH^+ + D \rightarrow Li^+ + HD$. In Figure 9 we report the total dissociation probabilities, together with the subreactive and reactive fluxes for the average collision energy of the wave packet of 1.0 eV and for the $n = 1$ initial vibrational state. The most striking result is that in both cases of isotopic substitutions

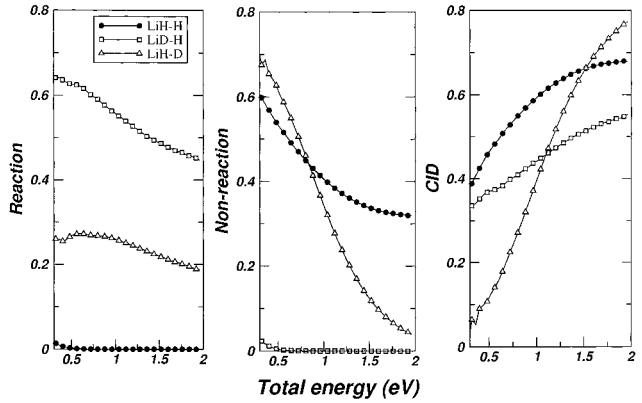

Figure 9. Total reaction, nonreaction, and CID probabilities for the three different isotopic variations examined in the text. The energy scale is the total energy and thus the dissociation threshold is the zero of the scale.

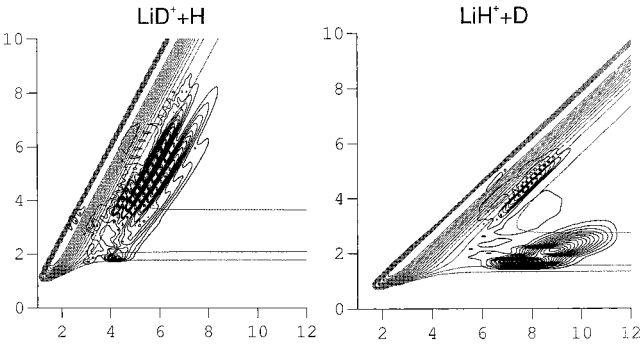

Figure 10. Probability density contour plots for the reaction of $LiD^+(n = 1) + H$ (on the left) and $LiH^+(n = 1) + D$ (on the right) at the end for the reaction (100 fs) for 1.0 eV of kinetic energy. Distances are in Å.

the reaction is highly enhanced and becomes, at least for LiD^+, the dominant process. This is most probably due to the greater ability for the product molecule HD to absorb the excess of translational energy with respect to the previous case of H_2. In the case of HD, in fact, the density of vibrational states is greater near the threshold, and the resulting potential energy surface has a less narrow exit channel (as a function of mass-scaled coordinates). An opposite behavior is registered for the nonreactive process, where, surprisingly, the isotopic substitution $LiH^+ \rightarrow LiD^+$ reduces significantly only the occurrence of the nonreactive transitions during collisions.

If we look at the probability density plot given in Figure 10, we see clearly that the distributions of the final wave packet are dramatically different from the one previously investigated for the nonisotopic reaction. This change can be justified in terms of the change of the skewing angle and of the enhanced capability of the product molecules to absorb the excess of energy because of the smaller energy spacings of their bound states. As we see in the left panel of Figure 10, the LiD^++H reacts and dissociates mostly in the product region, while the LiH^++D, shown in the right panel, continues, as the ligther case, to dissociate mostly in the reagent region.

As we have discussed before, we obtained from our calculations the state-to-state transition probabilities for the product H_2/HD molecules as they are exiting from the reaction region. The reaction, therefore, produces in all three cases a vibrationally hot diatomic molecule with an almost inverse Boltzmann population. A vibrationally hot hydrogen molecule was also found in the study, with the classical dynamics of the collinear neutral reaction LiH+H $\rightarrow$ H_2+Li done in ref 33.

5. Present Conclusions

We have used in the present study the TDSE approach to understand the dynamical behavior of the LiH^++H $\rightarrow$ H_2+Li^+-reaction, characterized by a very low threshold for the collision-induced dissociation, a feature we have related to the small binding energy of the reagent molecular partner. We found that a direct dynamics mechanism dominates the reaction when no rotational degrees of freedom are taken into account during the reactive collisions, as is the case in the present reduced dimensionality treatment.

The results showed a very low relative percentage of reaction and a pronounced tendency of the system to undergo, instead triatomic dissociation, an outcome that becomes the dominant process as soon as the collision energy is higher than a few eV. This result contrasts at first with a qualitative analysis of the underlying structure of the PES discussed in paper I, where we showed no activation barrier and a high exoergicity of it en route to the products. Isotopic substitutions further indicate that the narrowness of the exit channel is partially responsible for such behavior, while the lack of inelasticity in the exit channel invariably produces vibrationally hot products.

Furthermore, a marked vibrational enhancing of the CID probabilities has been found, in agreement with what had been noticed in previous work,[32] while a sort of memory effect of the initial wave function appears to be the cause of the shoulder structure in the total dissociation probabilities. Because of the simplified nature of the present collinear geometry, however, it still remains an open question whether this unexpected behavior will be confirmed when the full dimensionality of the problem is considered, i.e., when the rotation of the reacting molecular partner is included in the calculation via a full three-dimensional quantum mechanical treatment of the reactive process.

Given the very marked features exhibited by the present 2D calculations, however, and considering that the two extreme arrangements that we have examined here essentially provide the same physical picture, we do not expect that the full 3D reactive dynamics could totally eliminate the CID channel, which is seen here as the dominant process.

Acknowledgment. The financial support from the Italian Ministry for University and Research (MURST), from the University of Rome Research Commitee, and from the Max-Planck Research Society are gratefully acknowledged.

References and Notes

(1) de Bernardis, P.; Dubrovnich, V.; Encrenaz, P.; Maoli, R.; Masi, S.; Mastrantonio, G.; Melchiorri, B.; Melchiorri, F.; Signore, M.; Tanzilli, P. E. *Astron. Astrophys.* **1993**, *269*, 1.

(2) Maoli, R.; Melchiorri, F.; Tosti, D. *Astrophys. J.* **1994**, *425*, 372.

(3) Bougleux, E.; Galli, D. *Mon. Not. R. Astron. Soc.* **1997**, *288*, 638.

(4) Lepp, S.; Stancil, P. C. In *The Molecular Astrophysics of Star and Galaxies*; Hartquist, T. W., Williams, D. A., Eds.; Clarendon Press: Oxford, 1998.

(5) Puy, D.; Signore, M. *New Astron.* **1998**, *3*, 27.

(6) Galli, D.; Palla, F. In *The First Stars*; Weiss, A., Abel, T., Norman, M., Eds.; ESO/MPA Conference, 1999.

(7) Palla, F. In *Star Formation 1999*; Nakamoto, T., Ed.; Nobeyama Radio Observatory, 1999.

(8) Lepp, S.; Shull, J. M. *Astrophys. J.* **1984**, *280*, 465.

(9) Galli, D.; Palla, F. *Astron. Astrophys.* **1998**, *335*, 403.

(10) Bodo, E.; Gianturco, F. A.; Martinazzo, R.; Forni, A.; Famulari, A.; Raimondi, M. *J. Phys. Chem. A* **2000**, *104*, 11972.

(11) Bodo, E.; Gianturco, F. A.; Martinazzo, R.; Raimondi, M., in press.

(12) Gianturco, F. A.; Kumar, S.; Pathak, S. K.; Raimondi, M.; Sironi, M. *Chem. Phys.* **1997**, *215*, 239.

(13) Lee, H. S.; Lee, Y. S.; Jeung, G. *J. Phys. Chem. A* **1999**, *103*, 11080.

(14) Bodo, E.; Gianturco, F. A.; Martinazzo, R.; Raimondi, M. *Eur. Phys. J. D* **2001**, *15*, 321.
(15) Bodo, E.; Gianturco, F. A.; Martinazzo, R., in preparation.
(16) Levine, R. D.; Bernstein, R. B. *Molecular reaction dynamics and chemical reactivity*; Oxford University Press; Oxford, 1987.
(17) Diestler, D. J. In *Atom Molecule Collision Theory*; Bernstein, R. B., Ed,; Plenum Press: New York, 1979.
(18) Sakimoto, K.; Onda, K. *J. Chem. Phys.* **1994**, *100*, 1171.
(19) Sakimoto, K. *Chem. Phys. Lett.* **1996**, *248*, 414.
(20) Sakimoto, K., *Faraday Disc.* **1997**, *93*, 791.
(21) Onda, K.; Sakimoto, K. *J. Chem. Phys.* **1999**, *111*, 988.
(22) Sakimoto, K. *J. Chem. Phys.* **1999**, *110*, 11233.
(23) Sakimoto, K. *J. Chem. Phys.* **2000**, *112*, 5044.
(24) Nobusada, K.; Sakimoto, K. *J. Chem. Phys.* **1997**, *106*, 9078.
(25) Nobusada, K.; Sakimoto, K. *Chem. Phys. Lett.* **1998**, *288*, 311.
(26) Sakimoto, K. *Chem. Phys.* **1998**, *228*, 167.
(27) Kaye, J. A.; Kuppermann, A. *Chem. Phys. Lett.* **1981**, *78*, 546.
(28) Kaye, J. A.; Kuppermann, A. *Chem. Phys. Lett.* **1985**, *115*, 158.
(29) Kaye, J. A.; Kuppermann, A. *Chem. Phys.* **1988**, *125*, 279.
(30) Zhang, J. Z. H. *Theory and application of quantum molecular dynamics*; World Scientific: Singapore, 1999.
(31) Balakrishanan, N.; Kalyanaraman, C.; Sathyamurthy, N. *Phys. Rep.* **1997**, *280*, 79.
(32) Nobusada, K.; Sakimoto, K.; Onda, K. *Chem. Phys. Lett.* **1995**, *233*, 399.
(33) Clarke, N. J.; Sironi, M.; Raimondi, M.; Kumar, S.; Gianturco, F. A.; Buonomo, E.; Cooper, D. L. *Chem. Phys.* **1998**, *233*, 9.